Exploring the Chemical Space of G-Quadruplex Binders: Discovery of a Novel Chemotype Targeting the Human Telomeric Sequence

ARTICLE *in* JOURNAL OF MEDICINAL CHEMISTRY · NOVEMBER 2013

Impact Factor: 5.45 · DOI: 10.1021/jm401185b · Source: PubMed

Journal of Medicinal Chemistry

Article

pubs.acs.org/jmc

Exploring the Chemical Space of G-Quadruplex Binders: Discovery of a Novel Chemotype Targeting the Human Telomeric Sequence

Francesco Saverio Di Leva,[†] Pasquale Zizza,[‡] Chiara Cingolani,[‡] Carmen D'Angelo,[‡] Bruno Pagano,[§] Jussara Amato,[§] Erica Salvati,[‡] Claudia Sissi,[∥] Odra Pinato,[∥] Luciana Marinelli,[§] Andrea Cavalli,[†,⊥] Sandro Cosconati,[#] Ettore Novellino,[§] Antonio Randazzo,[*,§] and Annamaria Biroccio[‡]

[†]Department of Drug Discovery and Development, Istituto Italiano di Tecnologia, via Morego 30, 16163 Genova, Italy

[‡]Experimental Chemotherapy Laboratory, Regina Elena National Cancer Institute, 00158 Rome, Italy

[§]Department of Pharmacy, University of Naples "Federico II", via D. Montesano 49, I-80131 Napoli, Italy

[∥]Department of Pharmaceutical and Pharmacological Sciences, University of Padova, via Marzolo 5, 35131, Padova, Italy

[⊥]Department of Pharmacy and Biotechnology, Alma Mater Studiorum, University of Bologna, via Belmeloro 6, 40126 Bologna, Italy

[#]DiSTABiF, Second University of Naples, via Vivaldi 43, 81100 Caserta, Italy

Supporting Information

ABSTRACT: Recent findings have unambiguously demonstrated that DNA G-rich sequences can adopt a G-quadruplex folding in living cells, thus further validating them as crucial targets for anticancer therapy. Herein, to identify new potent G4 binders as antitumor drug candidates, we have targeted a 24-nt G4-forming telomeric sequence employing a receptor-based virtual screening approach. Among the best candidates, *in vitro* binding experiments allowed identification of three novel G4 ligands. Among them, the best compound features an unprecedented binding selectivity for the human telomeric DNA G-quadruplex with no detectable binding for other G4-forming sequences present at different genomic sites. This behavior correlates with the detected ability to generate DNA damage response in tumor cells at the telomeric level and efficient antiproliferative effect on different tumor cell lines at low micromolar concentrations.

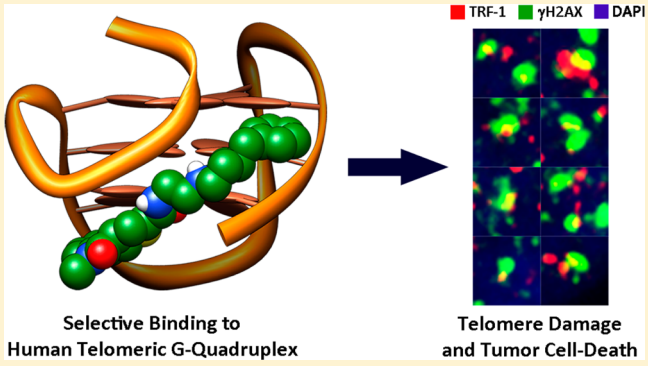

INTRODUCTION

The G-quadruplex (G4) is a four-stranded helical fold that is spontaneously adopted by guanine-rich (G-rich) sequences of DNA and RNA in the presence of cations. Several experiments have located these sequences in different critical positions of the human genome (mainly at the telomeric and gene promoter level).[1] Recently, the pioneering study by Balasubramanian and colleagues has unambiguously demonstrated G4 formation in living cells.[2] This work finally answers a long-standing research question in this field by demonstrating G4 existence in cells, substantiating both its biological relevance and its role as a target for anticancer therapy.

In the past decade, our research group has contributed to the study of G-quadruplex structural features[3] and, in recent years, to the discovery of small molecules able to interact with the G4, *in vitro*, and featuring antiproliferative properties.[4] In particular, our approach implied using a simple G4 forming sequence, namely, $[d(TGGGGT)]_4$,[4] as a working model to undertake a structure-based virtual screening (VS) campaign followed by physicochemical (mainly NMR and ITC) and biological studies to discover new G4 binders displaying good drug-like profiles and the ability to induce a DNA-damage response at telomeres of cancer cells.[4] Obviously, in these studies, the results of the structure-based VS were strongly influenced by the peculiar structural features of the chosen model. In this respect, while the $[d(TGGGGT)]_4$ G-quadruplex structure proved to be instrumental for the discovery of new G4 ligands featuring a groove binding mode, as opposed to the end-stacking one, its sequence does not correspond to the human telomeric sequence (tandem repeats of the sequence d(TTAGGG)). Moreover, it should be pointed out that G4 structures are conformationally promiscuous, since different topologies can be adopted depending on the nucleotide sequence considered, the experimental conditions (i.e., the monovalent cation used, K^+ or Na^+), and the physical method (NMR and X-ray crystallography) employed to solve the structure.[5]

All these considerations prompted us to move forward with our research by selecting a more biologically relevant telomeric G4 forming sequence as the target of our receptor-based VS

Received: August 2, 2013
Published: November 20, 2013

campaign, that is, the human telomeric G-quadruplex.[6] Results of this inspection led to the identification of a set of potential G4 ligands for which the *in vitro* binding was verified by fluorescence melting experiments and a fluorescent intercalator displacement assay. Interestingly, among the three chemotypes identified as true hits, one of them (compound **3** in Chart 1) displayed impressive G4 binding and stabilizing properties. A full physicochemical characterization allowed identification of the binding profile of these ligands. The subsequent profiling of the biological properties of the selected compounds demonstrated that **3** is outstandingly potent in inducing selective DNA damage at telomeres of cancer cells vs normal untransformed cells. In addition, this compound is endowed with efficient antiproliferative effect on several tumor cell lines.

Chart 1. Chemical Structures of the Newly Identified Human Telomeric G4 Binding Agents[a]

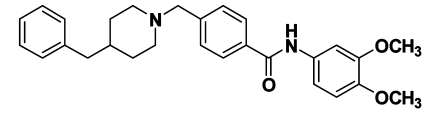

3553-0171
1

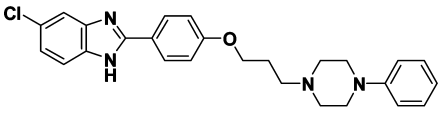

8017-3015
2

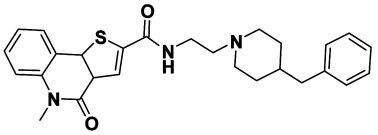

C066-3108
3

[a]TheChemDiv codes are reported in plain text. Numerals used in this paper are reported in bold.

RESULTS AND DISCUSSION

Virtual Screening. The plethora of structural data available for the G4 demonstrates that G-rich sequences can arrange by adopting a number of different topologies depending on the experimental conditions and selected sequences. Since we were mainly interested in finding new chemotypes that, by binding at the human telomeres, could induce a DNA-damage response and subsequent tumor cell death, we decide to target a G-quadruplex structure formed by the human telomeric sequence. Among all the DNA G4 structures having that sequence deposited in the Protein Data Bank, we looked for a G4 structure determined in the presence of the K^+ cation (which is more biologically relevant in the intracellular environment[7]) and possessing a single well-defined topology in solution, to warrant consistency between structure-based VS predictions and subsequent experimental verification of the binding properties of the computationally selected compounds.

This analysis resulted in the selection of the structure having PDB code 2GKU (herein referred to as Tel24).[8] This structure features a (3 + 1) core of the G4 topology where three strands are parallel and one is antiparallel. Such an arrangement allows for the formation of one narrow, one wide, and two medium grooves. Of these grooves, one is occupied by the double-chain-reversal loop; thus it is unavailable for ligand binding. As already outlined by Patel and colleagues, the above-described structural features of this G4 make it a "unique platform for structure-based anticancer drug design".[8]

In order to perform VS calculations on Tel24, we employed the software Autodock 4.2 (AD4.2),[9] which has proven to be effective in detecting nucleic-acid-binding small molecules.[4] Thus, AD4.2 was used to dock compounds from the commercially available ChemDiv database. Prior to docking calculations, the library was filtered by applying a Tanimoto similarity index of 0.7 to select a diversity set and then processed according to the ZINC protocol[10] to generate all the tautomeric and protomeric states for each compound. Finally, molecules having molecular weight lower than 250 Da or displaying exotic charges (e.g., ±5) were discarded leading to a subset of 18968 ligands. Given the presence of multiple druggable sites on Tel24 (three out of four grooves and a rather wide end-stacking surface), the docking search area was chosen to enclose the entire G-quadruplex structure. The VS results were sorted on the basis of the predicted ligand binding free energies (ΔG_{AD4}), which ranged from −4.14 to −13.58 kcal/mol. All the solutions with a ΔG_{AD4} greater than −10.0 kcal/mol and a cluster size population lower than 10 out of 100 individuals were discarded. The remaining solutions were visually inspected to discard all the compounds that were not predicted to establish tight contacts with Tel24 (i.e., Coulombic interactions with the phosphate backbone atoms). Indeed, these interactions can positively influence the stability of a ligand/G-quadruplex binary complex and even the proper orientation of a ligand with respect to the target DNA.[4] Subsequently, the remaining solutions were grouped based on their structural similarity to avoid structural redundancy, and the individuals with the lowest ΔG_{AD4} value within each group were finally selected. Finally, these compounds were carefully inspected for good geometries in the predicted binding pose. At the end of the visual inspection, 24 compounds corresponding to 0.13% of the docked ChemDiv database were considered for further investigations. Since six compounds were not available from the vendor, 18 compounds were purchased and tested in biophysical assays to evaluate their ability to bind the targeted G-quadruplex structure.[11]

Induced Thermal Stability. First, we employed a fluorescence quenching-based melting assay to evaluate the affinity of putative ligands for human telomeric G-quadruplex, by measuring the increase in the melting temperature (T_m) of the G-quadruplex induced by the presence of a ligand.[12,13] In order to perform the experiments, we used the same DNA target used in VS calculations (Tel24) in potassium-containing buffer. We recorded the ligand-induced variation of DNA melting temperature at three different ligands concentrations (Figure S1, Supporting Information) to evaluate any concentration-dependent increase of T_m. These experiments showed that 15 out of 18 compounds do not have the ability to significantly increase the T_m of the G-quadruplex, thus proving that they are nonbinders or weak binders of human telomeric G-quadruplex. On the other hand, these preliminary FRET melting experiments allowed the identification of three compounds (**1**−**3**) that increased the thermal stability of the Tel24 folded form and that could be considered potential lead compounds.

Therefore, we repeated again the FRET melting experiments for these three compounds by using a wider range of ligand concentrations. A ligand (ChemDiv code E240-0495, see Supporting Information) that turned out to not stabilize Tel24

dx.doi.org/10.1021/jm401185b | J. Med. Chem. 2013, 56, 9646−9654

was also used as negative control. As clearly shown in Figure 1a, **1** and **2** turned out to be quite poor G-quadruplex stabilizers.

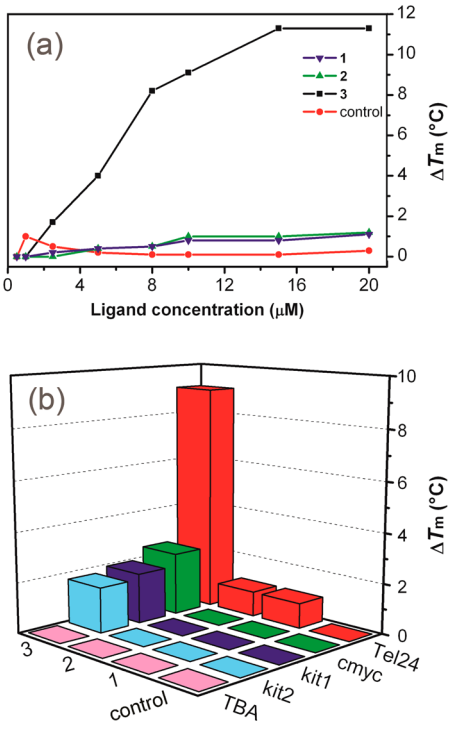

Figure 1. (a) Variation of the melting temperature (ΔT_m) of Tel24 induced by increasing concentrations of compounds **1**, **2**, and **3**. (b) T_m of different G-quadruplex-forming sequences induced by selected ligands (10 μM). Errors are ±0.2 °C. Control refers to compound E240-0495 (see Supporting Information).

Conversely, **3** showed relevant effects in the low micromolar range, inducing a considerable increase in the thermal stability of the G-quadruplex structure ($\Delta T_m \approx +11$ °C), thus suggesting a very strong interaction with the DNA. This also indicates that the VS probably succeeded in identifying a novel scaffold. In order to investigate the ability to discriminate among different G-quadruplex scaffolds, the same experimental assay was performed using different DNA sequences that form distinctive G-quadruplex structures. The results were impressive. Indeed, as shown in Figure 1b, they proved that **3** stabilizes to a large extent only Tel24, thus suggesting a high degree of selectivity for this compound. Interestingly, the other three tested compounds were not able to increase the thermal stability of any other G-quadruplex. Thus, off-target effects are rather reduced.

Fluorescent Intercalator Displacement Assay. The three tested compounds and the negative control were further analyzed by fluorescent intercalator displacement (FID) assay for their ability to displace the fluorescent probe thiazole orange (TO) from G-quadruplex folded sequences.[14] Indeed, this assay allows working with no labeled oligonucleotides, therefore avoiding possible interferences with ligand binding due to the presence of fluorophore and quencher. For compounds **1** and **2**, as well as for the negative control, no consistent reduction of the dye fluorescence signal associated with the DNA-bound TO was observed by increasing the amounts of the investigated ligands in solution (Figure 2 shows an example), thus indicating that they were not efficient in displacing TO from the G-quadruplex DNA. This could be due either to a weak

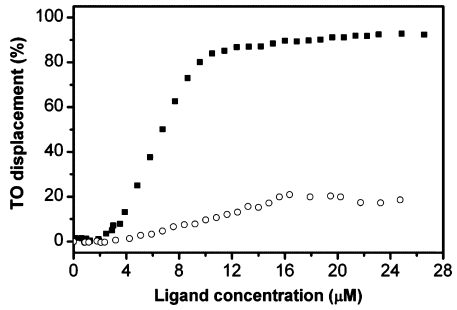

Figure 2. FID results obtained for **3** (filled squares) and for the negative control (open circles) with Tel24 using TO as fluorescent probe.

interaction with DNA or to an interaction with alternative binding sites that do not entail TO displacement. A different behavior was observed for **3**. Indeed, increments in the concentration of this compound succeeded in displacing the fluorescent probe, leading to an almost complete quenching of the fluorescence signal (Figure 2). Since this ligand does not have overlapping absorption bands with TO, this effect is surely due to the displacement of TO from DNA.

CD Spectroscopy. CD experiments were also carried out to evaluate whether (i) the G-quadruplex structure of Tel24 is retained upon **3** addition and (ii) the binding of the ligand alters its native folding topology. The investigated quadruplex-forming sequence showed the typical CD spectrum of the hybrid conformation (Figure 3), with a maximum around 290

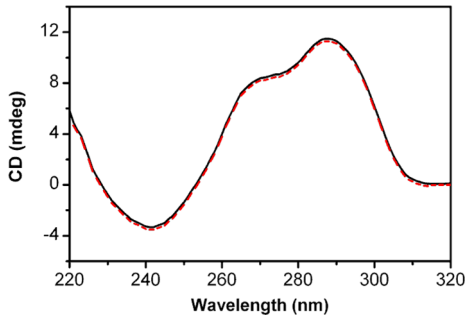

Figure 3. CD spectra of Tel24 before (black line) and after the addition of an excess of **3** (red dashed line).

nm, a shoulder centered around 270 nm, and a weak minimum around 240 nm.[15,16] The addition of **3** causes no relevant variations of DNA chiroptical signal, thus suggesting an almost overall conservation of the G-quadruplex structure as well as of its architecture. This result is particularly important in studies like this, since it allows us to confirm that the G-quadruplex structure used as target for the VS calculations does not change its native topology upon ligand interaction, different from what was observed for other G-quadruplex/ligand interactions.[17,18]

Nuclear Magnetic Resonance Spectroscopy. With the aim to obtain a more detailed picture of the interaction between **3** and the G-quadruplex formed by Tel24, we performed an NMR analysis. Particularly, the DNA has been titrated with **3** up to a 2:1 (ligand/G-quadruplex) stoichiometry. The addition of **3** to Tel24 caused a gradual change in chemical shift of some signals of the G-quadruplex. Furthermore, some signals of **3** could also be detected. These signals turned out to grow only in intensity and did not show any significant change in chemical shift values by increasing

dx.doi.org/10.1021/jm401185b | J. Med. Chem. 2013, 56, 9646−9654

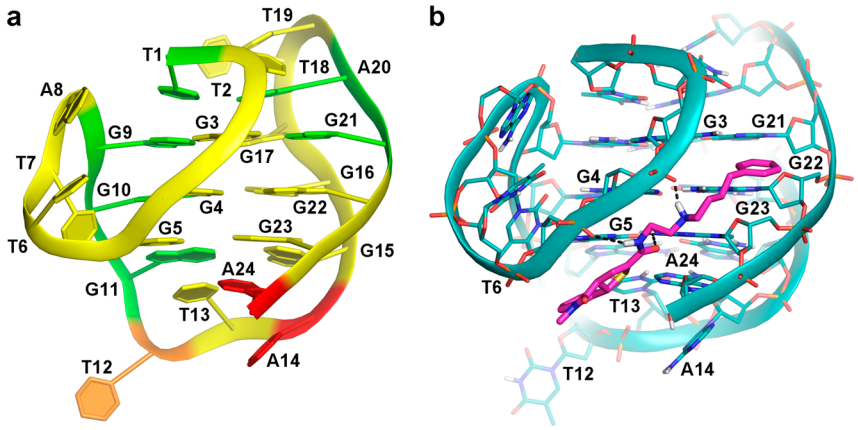

Figure 4. (a) Three-dimensional structure of Tel24 colored according to $\Delta\delta$ values measured in the presence of **3**: $\Delta\delta \leq 0.01$, green; $0.01 < \Delta\delta \leq 0.03$, yellow; $0.03 < \Delta\delta \leq 0.05$, orange; $\Delta\delta > 0.05$, red. (b) Binding mode of the best ranked binding pose of **3** to Tel24. The DNA is shown as cyan cartoon and lines, while the ligand is depicted as magenta sticks.

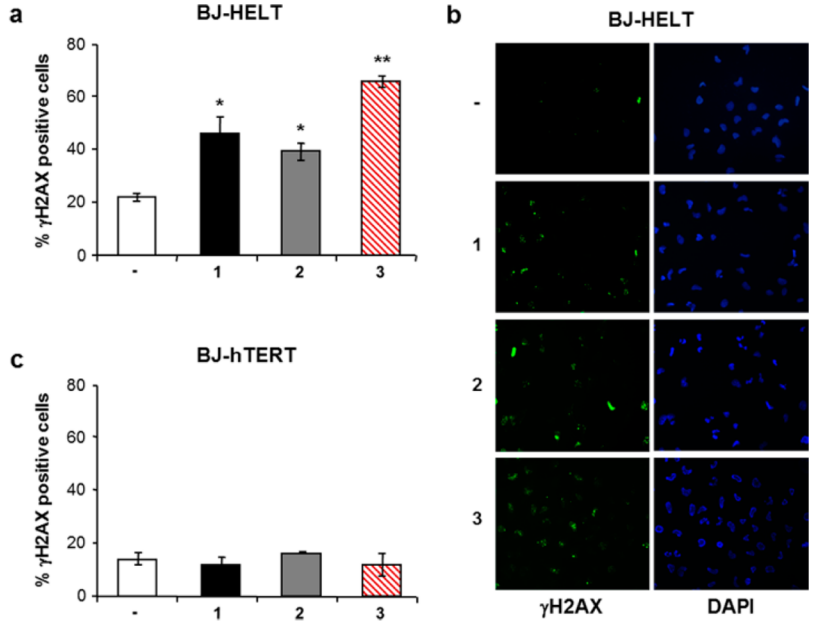

Figure 5. Analysis of DNA damage response by G-quadruplex ligands: (a, c) Transformed BJ-HELT fibroblasts (a) and their normal telomerized counterpart, BJ-hTERT (c), were grown for 24 h in the absence (Untreated) or in the presence of 1 μM of indicated compounds. DNA damage response was evaluated by immunofluorescence (IF) analysis by using an anti-γH2AX antibody and DAPI was used to mark nuclei. (a) Quantification of γH2AX-positive BJ-HELT fibroblasts. Histograms show the mean values ± SD of at least three independent experiments; p-values were calculated using the student's t test (*$p < 0.05$; **$p < 0.005$). (b) Representative images of IF analysis from panel a. Images were acquired using a Leica deconvolution microscope (magnification 40×). (c) Quantification of γH2AX-positive BJ-hTERT fibroblasts. Data represent means ± SD of three independent experiments.

ligand concentration. These results clearly suggest that **3** binds the G-quadruplex in a fast process on the NMR time scale. In order to evaluate the specific DNA residues involved in the interaction with **3**, a difference of resonances of the aromatic protons of the complexed DNA and the uncomplexed one has been done, calculating the corresponding $\Delta\delta$ values. In particular, $\Delta\delta$ values were used to highlight the residues of the G-quadruplex structure involved in the interaction with **3**. Different colors (green, yellow, orange, and red) were used to outline different ranges of $\Delta\delta$ values ($\Delta\delta \leq 0.01$, $0.01 < \Delta\delta \leq 0.03$, $0.03 < \Delta\delta \leq 0.05$, $\Delta\delta > 0.05$, respectively). Figure 4a shows that **3** interacts more with residues T12−A14, including the residues G22−A24 and G3−G5. Interestingly, the T6-T7-A8 and T18-T19 loops, along with the strand G15−G17, are also interesting for the binding. These data clearly indicate that **3** does not possess a unique binding pose. However, the data provided by NMR experiments are in good agreement with VS results. Indeed, in the best predicted docking pose (Figure 4b), **3** stacks with its planar scaffold at the 3′ region of Tel24, primarily interacting with residues T13, A14, and A24. Furthermore, the positively charged branch of **3** extends into the medium groove, which is accessible for ligand binding. Here, the amide group of the ligand donates and accepts two H-bonds with the phosphate group of G5 and the amino group of G23, respectively. Moreover, the protonated nitrogen atom of the piperazinyl ring salt bridges with the phosphate group of G4. Finally, the benzyl moiety is predicted to establish parallel displaced interactions with residues G3 and G22.

Biological Activity. Specific biological assays have been performed on the best compounds of the series. First, we

dx.doi.org/10.1021/jm401185b | J. Med. Chem. 2013, 56, 9646−9654

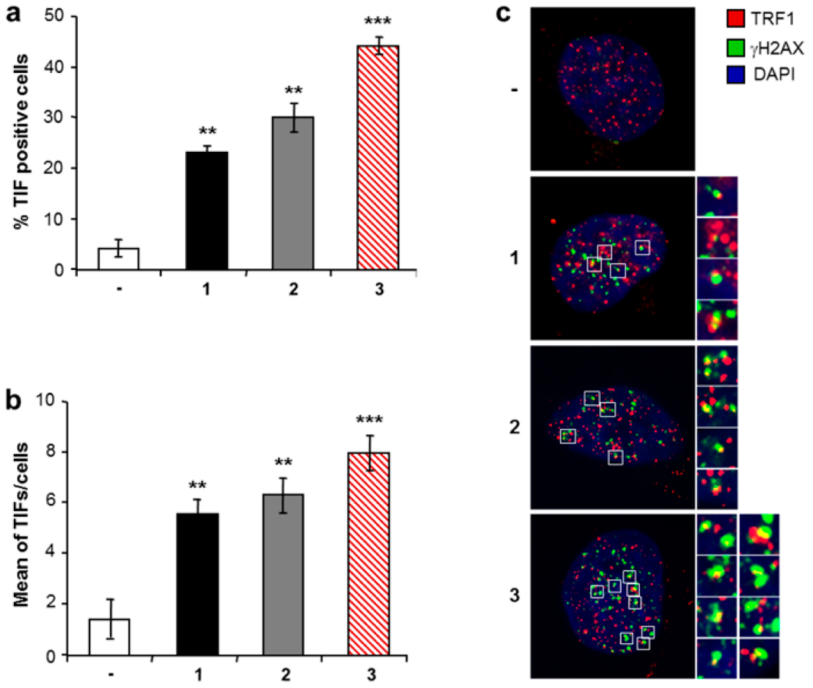

Figure 6. Analysis of telomere damage by G-quadruplex ligands: BJ-HELT fibroblasts were grown in the absence (−) or in the presence of 1 μM of the indicated compounds and then processed for IF analysis using antibodies against γH2AX and TRF1 to mark DNA damage and telomeres, respectively; DAPI staining was used to mark nuclei. Quantification of TIF-positive cells (a) and mean number of TIFs per nucleus (b) in the indicated conditions. Data are means ± SD of three independent experiments; *p*-values were calculated using the student's *t* test (**$p < 0.005$; ***$p < 0.001$). (c) Representative IF images from panels a and b. Enlarged views of TIFs are reported on the right of each picture. The images were acquired by using a Leica deconvolution microscope (magnification 63×).

evaluated the ability of the different ligands to directly uncap telomeres. To this aim, human transformed (BJ-HELT) and normal telomerized (BJ-hTERT) fibroblasts were exposed to 1 μM concentration of compounds **1**, **2**, and **3** for 24 h, and activation of DNA damage response was analyzed (Figure 5). Immunofluorescence (IF) analysis performed to evaluate the phosphorylation of H2AX (γH2AX), a hallmark of DNA double-strand break,[19] showed that all the compounds activated a DNA damage response pathway in the transformed fibroblasts, and compound **3** was the most potent DNA damage inducer, triggering about 60% of cells positive for γH2AX (Figure 5a,b). Interestingly, all the tested compounds used at the same drug concentration did not produce any activation of H2AX in normal telomerized fibroblasts (Figure 5c), indicating that the ligands are selective for transformed cells. To test whether γH2AX was phosphorylated in response to dysfunctional telomeres, double IF experiments were performed. Deconvolution microscopy showed that some of the damaged foci induced by compounds colocalized with TRF1, an effective marker for interphase telomeres, forming the so-called telomere-dysfunction induced foci (TIFs)[20] (Figure 6), concluding that the tested compounds caused telomere damage.

Consistent with the data reported in Figure 5a, results from quantitative analysis revealed that **3** was the most potent telomere damage inducer, increasing the percentage of TIF-positive cells up to 50% (Figures 6a,c), with a mean of about eight TIFs per nucleus (Figure 6b). The experiments performed above on the three different compounds have identified **3** as the most promising telomere damaging agent, warranting further studies. Therefore, we decided to evaluate the effect of **3** on tumor cell survival by clonogenic assay, which is the most valid test to measure *in vitro* the fraction of cells that can survive after drug treatment. The analysis, performed on three cancer cell lines of different histotype, revealed that **3** was able to inhibit the cell survival of all the analyzed tumor lines (Figure 7a) in a dose-dependent manner, with the IC_{50} values ranging from about 1 to 3 μM. In contrast, the viability of normal fibroblasts (BJ-hTERT), assayed by MTT, was unaffected by the treatment even at the highest drug concentration (Figure 7a). Consistent with these results, cell cycle analysis performed from day 4 to 6 of treatment revealed that **3** induced a time-dependent accumulation of cells in the sub-G1 compartment (Figure 7b), indicative of apoptosis. Annexin staining performed at day 5 of treatment revealed that **3** induced about 40% of annexin-V positive/PI negative cells, confirming that this compound triggers apoptotic cell death (Figure 7b, insets).

■ CONCLUSIONS

The recent advances in the G-quadruplexes research field further support the crucial role played by these DNA motifs in living organisms, validating them as key targets in anticancer therapy.[2] However, none of the G4 ligands developed so far has made it through the drug discovery pipeline due to poor drug-like properties, poor selectivity profile, or both. This is strongly encouraging researchers to make further efforts in the identification of G4 binding agents as potential anticancer drugs. Herein, the application of structure-based VS succeeded in the identification of a novel chemotype as a potent and selective binder of the human telomeric G4. The *in vitro* G4 binding properties of these compounds were indeed proven by a large panel of biophysical assays. In particular, melting and fluorescent intercalator displacement experiments revealed that

dx.doi.org/10.1021/jm401185b | J. Med. Chem. 2013, 56, 9646−9654

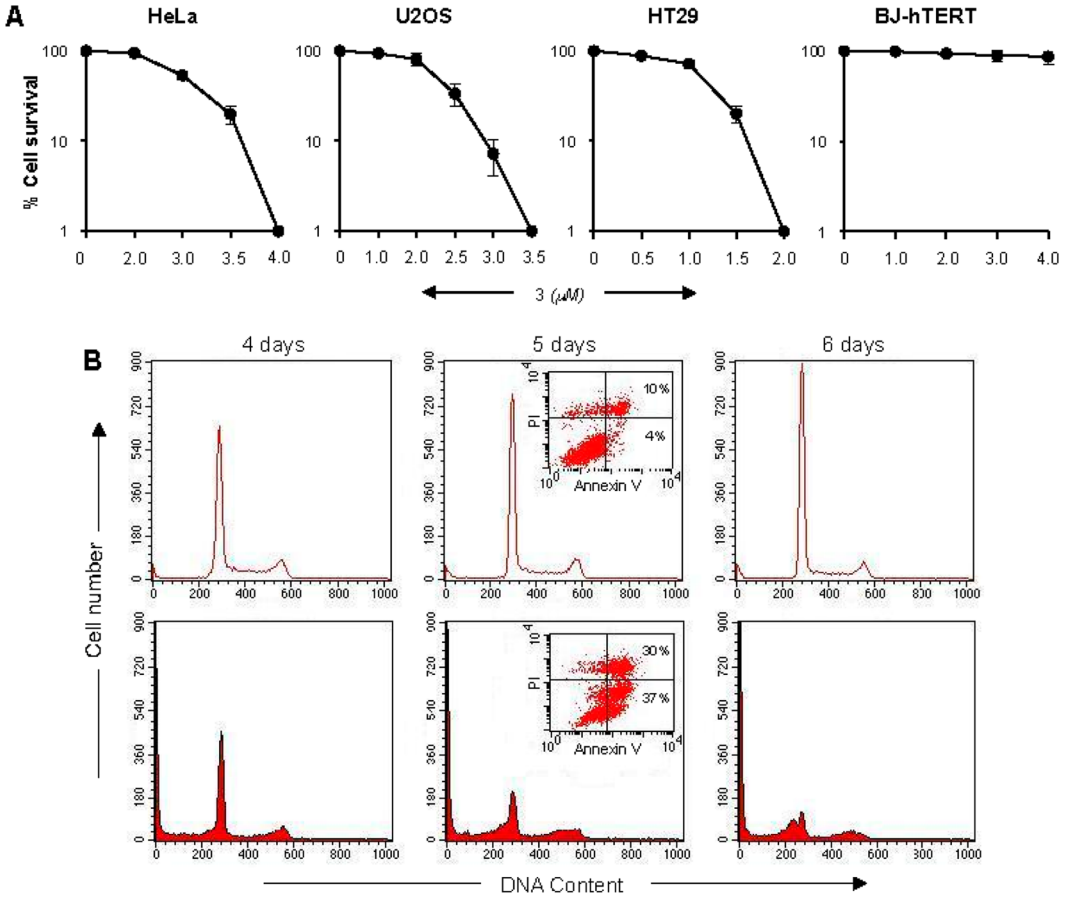

Figure 7. Analysis of antitumoral activity of **3**: (a) HeLa cervix adenocarcinoma, U2OS osteosarcoma, HT29 colorectal adenocarcinoma, and BJ-hTERT normal fibroblast cell lines were treated with the indicated doses of **3** for 4 days, and the cell survival was evaluated. Surviving fractions were calculated as the ratio of absolute survival of the treated samples/absolute survival of the control samples. Data are means ± SD of the three independent experiments. (b) Cell cycle evaluation of HT29 cell growth in the absence (upper panels) or in the presence (lower panels) of 2 μM compound **3**. Flow cytometry analyses after PI staining were performed at 4, 5, and 6 days of treatment. Insets: evaluation of apoptosis by biparametric dot plots analysis of PI vs annexin V staining was performed at day 5 of treatment.

compound **3** features enhanced affinity and selectivity toward the human telomeric DNA sequence vs other G4 forming sequences present along the human genome (e.g., *kit* and *myc* gene promoters). Furthermore, CD experiments demonstrated that the binding of **3** to the human telomeric G4 does not alter the overall DNA architecture, indicating a high degree of complementarity between **3** and the native topology of the target. In perfect line with *in vitro* assays, the subsequent biological characterization demonstrated that **3** is able to induce DNA damage at telomeres in cancer cells and not in untransformed ones. Further analyses revealed that this ligand is able to inhibit cell survival on three different cancer cell lines at low micromolar concentrations, eventually triggering apoptotic cell death. This study thus provides a new promising prototype for the design of selective and biologically effective drug-like G4 ligands, thus paving the way to the development of new anticancer drug candidates.

EXPERIMENTAL METHODS

Virtual Screening. The Autodock 4.2 (AD4.2)[9] software package, as implemented through the graphical user interface called AutoDockTools (ADT)[21] was used to dock small molecules to the G-quadruplex structure. The DNA was prepared using published coordinates (PDB 2GKU).[8] Preparation of the DNA and ligands structures for docking calculations was attained according to the parametrization suggested by Neidle and co-workers.[22] Thus, point charges were assigned to the DNA according to the Amber94 force field,[23] and all other atom values were generated automatically by ADT. The docking area was assigned so as to enclose the entire G-quadruplex and centered on the center of mass of the macromolecule. A grid of 123 × 123 × 123 Å^3 with 0.375 Å spacing was thus calculated around the docking area for 12 ligand atom types using Autogrid4.2. These atom types were sufficient to describe all atoms in the ChemDiv database. For VS, the library was filtered by applying a pairwise Tanimoto similarity index of 0.7 as a threshold and then processed using the ZINC database server (http://zinc.docking.org)[10] to take into account the different protomeric and tautomeric states of each compound. The database was then further filtered to discard molecules having molecular weight lower than 250 Da or displaying exotic charges (e.g., ±5) leading to a subset of 18968 ligands. All the ligands were then converted in the AutoDock format file (.pdbqt). For each ligand, 100 separate docking calculations were performed. Each docking calculation consisted of 10 million energy evaluations using the Lamarckian genetic algorithm local search (GALS) method. The GALS method evaluates a population of possible docking solutions and propagates the most successful individuals from each generation into the subsequent generation of possible solutions. A low-frequency local search according to the method of Solis and Wets is applied to docking trials to ensure that the final solution represents a local minimum. All the dockings described in this paper were performed with a population size of 150, and 300 rounds of Solis and Wets local search were applied with a probability of 0.06. A mutation rate of 0.02 and a crossover rate of 0.8 were used to generate new docking trials for subsequent generations, and the best individual from each generation

dx.doi.org/10.1021/jm401185b | J. Med. Chem. 2013, 56, 9646−9654

was propagated to the next generation. The docking results from each of the eight calculations were clustered on the basis of root-mean-square deviation (rmsd) between the Cartesian coordinates of the atoms and were ranked on the basis of free energy of binding. The top-ranked compounds were visually inspected for good chemical geometry.

Oligonucleotide Sequences. Synthetic oligonucleotides were provided by Biosense (Belgium) as HPLC purified material and used with no further purification. In particular the following DNA sequences have been used: c-myc (5′-TGA-GGG-TGG-GGA-GGG-TGG-GGA-AGG-3′); kit-1 (5′-AGG-GAG-GGC-GCT-GGG-AGG-AGG-G-3′); kit-2 (5′-CGG-GCG-GGC-GCG-AGG-GAG-GGG-3′); TBA (5′-GGT-TGG-TGT-GGT-TGG-3′); Tel24 (5′-TTG-GGT-TAG-GGT-TAG-GGT-TAG-GGA-3′).

Compound Purity. The selected compounds were purchased by ChemDiv (see Table S1, Supporting Information). Their purity was assessed using reversed-phase high-performance liquid chromatography (HPLC) analyses using Shimadzu C18, 5 μm (150 mm × 4.6 mm) column. The elution was performed with a 1.0 mL/min flow rate using a linear gradient from 0 to 100% methanol in water over 30 min. The detection was performed at 210 nm. The purity was also tested with high-performance liquid chromatography−mass spectrometry (HPLC−MS) analyses performed on an Agilent 1200 series (Agilent Technologies, Santa Clara, CA, USA) equipped with an Agilent 6110 series LC/MS quadrupole, using a Phenomenex Luna C18, 5 μm (150 mm × 4.6 mm) column. The elution was performed with a 1.0 mL/min flow rate using a linear gradient from 0 to 90% acetonitrile in water over 20 min. Detection was performed at 210 nm. The purity of compounds was higher than 98.0%. The active compounds (**1**, **2**, and **3**) were further investigated by ^{1}H NMR, and the spectra are reported in Supporting Information (Figure S3).

Fluorescence Melting Experiments. Melting experiments were performed in a 96-wells plate using a Roche LightCycler 480. The excitation source was set at 488 nm, and the fluorescence emission was recorded at 520 nm. Target DNA molecules were labeled with DABCYL at 5′-end and fluorescein at 3′-end. Mixtures (20 μL) contained 0.25 μM target DNA and variable concentrations of tested derivatives in 50 mM potassium buffer (10 mM LiOH, 50 mM KCl, pH 7.4, with H_3PO_4). They were first denatured by heating to 95 °C for 5 min and then slowly cooled overnight. Then temperature was increased up to 90 °C at 0.2 °C/min and again lowered at the same rate to 30 °C. Recordings were taken during both these melting and annealing reactions to check for hysteresis. T_m values were determined from the first derivatives of the melting profiles using the Roche LightCycler software. Each curve was repeated at least three times and errors were ±0.2 °C.

Fluorescent Intercalator Displacement (FID) Assay. FID experiments were performed using a PerkinElmer VICTOR plate reader (96-well plates) or a PerkinElmer 50LS. To reaction mixtures containing 0.6 μM of target DNA and 1.2 μM of thiazole orange (TO) were added increasing concentrations of tested derivatives in 10 mM Tris, 50 mM KCl, pH 7.4. Changes in fluorescence emission were recorded. The percentage of TO displacement was calculated (TO displacement = $100 - [(F/F_0) \times 100]$, F_0 being the fluorescence F before addition of ligand) and plotted as a function of compound concentration. Each assay was repeated at least three times in triplicate.

CD Measurements. CD spectra were recorded at 25 °C on a Jasco J-715 spectropolarimeter equipped with a Peltier-type temperature control system (model PTC-348WI) and calibrated with an aqueous solution of 0.06% D-10-(1)-camphorsulfonic acid at 290 nm. CD spectra of previously annealed DNA solutions (40 μM) were recorded between 220 and 320 nm in the absence or presence of an excess of **3** in 10 mM Tris-HCl, 50 mM KCl, pH 7.4, using 1 mm path-length cuvettes and were averaged over three scans. Buffer baseline was subtracted from each spectrum. A time constant of 4 s, a 2 nm bandwidth, and a scan rate of 20 nm min^{-1} were used to acquire the data.

Nuclear Magnetic Resonance Experiments. The G-quadruplex NMR samples were prepared at a concentration of 2 mM in 0.6 mL (H_2O/D_2O 9:1) buffer solution having 10 mM KH_2PO_4, 70 mM KCl, 0.2 mM EDTA, pH 7.0. NMR spectra were recorded with Varian UnityINOVA 700 MHz spectrometer. ^{1}H chemical shifts were referenced relative to external sodium 2,2-dimethyl-2-silapentane-5-sulfonate (DSS). One-dimensional proton spectra of the sample in H_2O were recorded using pulsed-field gradient DPFGSE[24] for H_2O suppression. The NMR data were processed on iMAC running iNMR software (www.inmr.net).

Cells and Culture Conditions. BJ fibroblasts expressing hTERT (BJ-hTERT) or hTERT plus SV40 early region (BJ-HELT) and human colorectal adenocarcinoma (HT29) were obtained as reported in a previous work.[25] Human epithelial carcinoma cell line (HeLa) and human osteosarcoma (U2OS) were purchased from ATCC. All the lines were grown in Dulbecco's modified Eagle medium (D-MEM, Invitrogen Carlsbad, CA, USA) supplemented with 10% fetal calf serum, 2 mM L-glutamine, and antibiotics.

Immunofluorescence. Immunofluorescence (IF) was performed as previously described.[25] Briefly, cells were fixed in 2% formaldehyde and permeabilized in PBS plus 0.25% Triton X-100 for 5 min at room temperature. For immunolabeling, cells were incubated with primary antibody (RT, 2 h), washed twice in PBS, and finally incubated with the secondary antibodies (RT, 1 h). The following primary antibodies were used: rabbit polyclonal anti-TRF1 antibody (Abcam Ltd., Cambridge, U.K.); mouse monoclonal anti-γH2AX antibody (Upstate, Lake Placid, NY). The following secondary antibodies were used: TRITC-conjugated goat anti-rabbit, FITC-conjugated goat anti-mouse (Jackson Lab.). Nuclei were immunostained with DAPI. Fluorescence signals were recorded by using a Leica DMIRE2 microscope equipped with a Leica DFC 350FX camera and elaborated by Leica FW4000 deconvolution software (Leica, Solms, Germany). For quantitative analysis of γH2AX positivity, 200 cells on triplicate slices were scored. For TIF analysis, a single plane was analyzed, and 30 γH2AX-positive cells were scored. Cells with at least four colocalizations (γH2AX/TRF1) were considered as TIF-positive.

Clonogenic Assay. Cells were seeded in 60 mm Petri dishes (Nunc, MasciaBrunelli, Milan, Italy) at a density of 5×10^2 cells per dish and, 24 h later, exposed to the indicated treatments. After 4 days, cell colony-forming capability was determined as described in a previous work.[26]

MTT Assay. BJ-hTERT cells were seeded at 3×10^3 cells/well in a 96-well plate (Nunc, MasciaBrunelli, Milan, Italy) and, 24 h later, treated with 0, 1, 2, or 3 μM of compound **3**. After 4 days, MTT solution (Sigma-Aldrich, 5 mg/mL in phosphate-buffered saline) was added (20 μL/well), and the plate was incubated for additional 4 h at 37 °C. The purple formazan crystals were dissolved in 200 μL of isopropanol per well. OD at 540 nm was determined on microplate reader.

Flow Cytometric Analysis. The cell cycle analysis was performed by flow cytometry. Cells were washed in PBS and fixed in 70% ethanol; 1×10^6 cells were centrifuged and resuspended in a staining solution (50 μg/mL PI, 75 KU/mL RNase A in PBS) for 30 min at room temperature in the dark and analyzed by flow cytometry using FACScalibur (Becton-Dickinson, San Jose, CA, USA). For each analysis 20000 events were collected. Cell cycle distribution and percentage of apoptotic cells was analyzed using Cell Quest (BDIS) and ModFit LT (Verity Software House, Topsham, ME). Apoptosis was analyzed by flow cytometric analysis of annexin V staining. Annexin V−FITC vs PI assay (Vibrant apoptosis assay, V-13242, Molecular Probes, Eugene, OR, USA) was performed as previously described.[27] Briefly, adherent cells were harvested, incubated (1×10^6 cells/mL) with annexin V−FITC and PI for 15 min at room temperature in the dark, and analyzed by flow cytometry. The data are presented as biparametric dot plots showing PI red fluorescence vs annexin V−FITC green fluorescence.

Statistical Analysis. The experiments have been repeated from three to five times, and the results obtained are presented as means ± standard deviation (SD). Significant changes were assessed by using Student's t test for unpaired data, and p values of <0.05 were considered significant.

■ ASSOCIATED CONTENT

Supporting Information

Vendor codes for each tested compound, thermal stability experiments, and ^{1}H NMR spectra of active compounds. This material is available free of charge via the Internet at http://pubs.acs.org.

■ AUTHOR INFORMATION

Corresponding Author

*E-mail: antonio.randazzo@unina.it. Tel: +39-081-678514.

Author Contributions

The manuscript was written through contributions of all authors. All authors have given approval to the final version of the manuscript. F.S.D.L. and P.Z. contributed equally.

Notes

The authors declare no competing financial interest.

■ ACKNOWLEDGMENTS

This work was supported by the Italian Institute of Technology (IIT), Italian Association for Cancer Research (A.I.R.C. No. 11567 and No. 11947), and Italian MIUR (PRIN 2009).

■ ABBREVIATIONS

G4, G-quadruplex; VS, virtual screening; NMR, nuclear magnetic resonance; ITC, isothermal titration calorimetry; AD4.2, Autodock 4.2; ADT, AutoDockTools; GALS, Lamarckian genetic algorithm local search; FID, fluorescent intercalator displacement; TO, thiazole orange; IF, immunofluorescence; SD, standard deviation; ΔG_{AD4}, Autodock-predicted binding free energy; T_m, melting temperature; TIF, telomere-dysfunction induced foci

■ REFERENCES

(1) (a) Sandell, L. L.; Zakian, V. A. Loss of a yeast telomere: Arrest, recovery and chromosome loss. *Cell* **1993**, *75*, 729−739. (b) De Cian, A.; Lacroix, L.; Douarre, C.; Temime-Smaali, N.; Trentesaux, C.; Riou, J.-F.; Mergny, J.-L. Targeting telomeres and telomerase. *Biochimie* **2008**, *90*, 131−155. (c) Paeschke, K.; Simonsson, T.; Postberg, J.; Rhodes, D.; Lipps, H. J. Telomere end-binding proteins control the formation of G-quadruplex DNA structures *in vivo*. *Nat. Struct. Mol. Biol.* **2005**, *12*, 847−854.

(2) Biffi, G.; Tannahill, D.; McCafferty, J.; Balasubramanian, S. Quantitative visualization of DNA G-quadruplex structures in human cells. *Nat. Chem.* **2013**, *5*, 182−186.

(3) (a) Virno, A.; Mayol, L.; Ramos, A.; Fraternali, F.; Pagano, B.; Randazzo, A. Structural insight into the hTERT intron 6 sequence d(GGGGTGAAAGGGG) from ^{1}H-NMR study. *Nucleosides, Nucleotides Nucleic Acids* **2007**, *26*, 1133−11337. (b) Virno, A.; Randazzo, A.; Giancola, C.; Bucci, M.; Cirino, G.; Mayol, L. A novel thrombin binding aptamer containing a G-LNA residue. *Bioorg. Med. Chem.* **2007**, *15*, 5710−5718. (c) Limongelli, V.; De Tito, S.; Cerofolini, L.; Fragai, M.; Pagano, B.; Trotta, R.; Cosconati, S.; Marinelli, L.; Novellino, E.; Bertini, I.; Randazzo, A.; Luchinat, C.; Parrinello, M. The G-triplex DNA. *Angew. Chem., Int. Ed.* **2013**, *52*, 2269−2273.

(4) (a) Martino, L.; Virno, A.; Pagano, B.; Virgilio, A.; Di Micco, S.; Galeone, A.; Giancola, C.; Bifulco, G.; Mayol, L.; Randazzo, A. Structural and thermodynamic studies of the interaction of distamycin A with the parallel quadruplex structure $[d(TGGGGT)]_4$. *J. Am. Chem. Soc.* **2007**, *129*, 15950−15956. (b) Cosconati, S.; Marinelli, L.; Trotta, R.; Virno, A.; Mayol, L.; Novellino, E.; Olson, A. J.; Randazzo, A. Tandem application of virtual screening and NMR experiments in the discovery of brand new DNA quadruplex groove binders. *J. Am. Chem. Soc.* **2009**, *131*, 16336−16337. (c) Cosconati, S.; Marinelli, L.; Trotta, R.; Virno, A.; De Tito, S.; Romagnoli, R.; Pagano, B.; Limongelli, V.; Giancola, C.; Baraldi, P. G.; Mayol, L.; Novellino, E.; Randazzo, A. Structural and conformational requisites in DNA quadruplex groove binding: Another piece to the puzzle. *J. Am. Chem. Soc.* **2010**, *132*, 6425−64333. (d) Trotta, R.; De Tito, S.; Lauri, I.; La Pietra, V.; Marinelli, L.; Cosconati, S.; Martino, L.; Conte, M. R.; Mayol, L.; Novellino, E.; Randazzo, A. *Biochimie* **2011**, *93*, 1280−1287. (e) Cosconati, S.; Rizzo, A.; Trotta, R.; Pagano, B.; Iachettini, S.; De Tito, S.; Lauri, I.; Fotticchia, I.; Giustiniano, M.; Marinelli, L.; Giancola, C.; Novellino, E.; Biroccio, A.; Randazzo, A. Shooting for selective drug-like G-quadruplex binders: evidence for telomeric DNA damage and tumor cell death. *J. Med. Chem.* **2012**, *55*, 9785−9792.

(5) Dai, J.; Carver, M.; Yang, D. Polymorphism of human telomeric quadruplex structures. *Biochimie* **2008**, *90*, 1172−1183.

(6) Alcaro, S.; Musetti, C.; Distinto, S.; Casatti, M.; Zagotto, G.; Artese, A.; Parrotta, L.; Moraca, F.; Costa, G.; Ortuso, F.; Maccioni, E.; Sissi, C. Identification and characterization of new DNA G-quadruplex binders selected by a combination of ligand and structure-based virtual screening approaches. *J. Med. Chem.* **2013**, *56*, 843−855.

(7) (a) Balagurumoorthy, P.; Brahmachari, S. K. Structure and stability of human telomeric sequence. *J. Biol. Chem.* **1994**, *269*, 21858−21869. (b) Ying, L. M.; Green, J. J.; Li, H. T.; Klenerman, D.; Balasubramanian, S. Studies on the structure and dynamics of the human telomeric G-quadruplex by single-molecule fluorescence resonance energy transfer. *Proc. Natl. Acad. Sci. U.S.A.* **2003**, *100*, 14629−14634. (c) Redon, S.; Bombard, S.; Elizondo-Riojas, M. A.; Chottard, J. C. Platinum cross-linking of adenines and guanines on the quadruplex structures of the $AG_3(T_2AG_3)_3$ and $(T_2AG_3)_4$ human telomere sequences in Na^+ and K^+ solutions. *Nucleic Acids Res.* **2003**, *31*, 1605−1613. (d) Phan, A. T.; Patel, D. J. Two-repeat human telomeric d(TAGGGTTAGGGT) sequence forms interconverting parallel and antiparallel G-quadruplexes in solution: distinct topologies, thermodynamic properties, and folding/unfolding kinetics. *J. Am. Chem. Soc.* **2003**, *125*, 15021−15027.

(8) Luu, K. N.; Phan, A. T.; Kuryavyi, V.; Lacroix, L.; Patel, D. J. Structure of the human telomere in K+ solution: An intramolecular (3 + 1) G-quadruplex scaffold. *J. Am. Chem. Soc.* **2006**, *128*, 9963−9970.

(9) (a) Morris, G. M.; Goodsell, D. S.; Halliday, R. S.; Huey, R.; Hart, W. E.; Belew, R. K.; Olson, A. J. Automated docking using a Lamarckian genetic algorithm and an empirical binding free energy function. *J. Comput. Chem.* **1998**, *19*, 1639−1662. (b) Huey, R.; Morris, G. M.; Olson, A. J.; Goodsell, D. S. A semiempirical free energy force field with charge-based desolvation. *J. Comput. Chem.* **2007**, *28*, 1145−1152.

(10) Irwin, J. J.; Shoichet, B. K. ZINC − A Free Database of Commercially Available Compounds for Virtual Screening. *J. Chem. Inf. Model.* **2005**, *45*, 177−182.

(11) Pagano, B.; Cosconati, S.; Gabelica, V.; Petraccone, L.; De Tito, S.; Marinelli, L.; La Pietra, V.; Di Leva, F. S.; Lauri, I.; Trotta, R.; Novellino, E.; Giancola, C.; Randazzo, A. State-of-the-art methodologies for the discovery and characterization of DNA G-quadruplex binders. *Curr. Pharm. Des.* **2012**, *18*, 1880−1899.

(12) Mergny, J. L.; Maurizot, J. C. Fluorescence resonance energy transfer as a probe for G-quartet formation by a telomeric repeat. *ChemBioChem* **2001**, *2*, 124−132.

(13) Giancola, C.; Pagano, B. Energetics of ligand binding to G-quadruplexes. *Top. Curr. Chem.* **2013**, *330*, 211−242.

(14) Monchaud, D.; Allain, C.; Teulade-Fichou, M. P. Development of a fluorescent intercalator displacement assay (G4-FID) for establishing quadruplex-DNA affinity and selectivity of putative ligands. *Bioorg. Med. Chem. Lett.* **2006**, *16*, 4842−4845.

(15) Vorlíčková, M.; Kejnovská, I.; Sagi, J.; Renčiuk, D.; Bednářová, K.; Motlová, J.; Kypr, J. Circular dichroism and guanine quadruplexes. *Methods* **2012**, *57*, 64−75.

(16) (a) Masiero, S.; Trotta, R.; Pieraccini, S.; De Tito, S.; Perone, R.; Randazzo, A.; Spada, G. P. A non-empirical chromophoric interpretation of CD spectra of DNA G-quadruplex structures. *Org. Biomol. Chem.* **2010**, *8*, 2683−2692. (b) Karsisiotis, A. I.; Hessari, N. M.; Novellino, E.; Spada, G. P.; Randazzo, A.; Webba da Silva, M. Topological characterization of nucleic acid G-quadruplexes by UV absorption and circular dichroism. *Angew. Chem., Int. Ed.* **2011**, *50*,

10645−10646. (c) Randazzo, A.; Spada, G. P.; da Silva, M. W. Circular dichroism of quadruplex structures. *Top. Curr. Chem.* **2013**, *330*, 67−86.
(17) Martino, L.; Pagano, B.; Fotticchia, I.; Neidle, S.; Giancola, C. Shedding light on the interaction between TMPyP4 and human telomeric quadruplexes. *J. Phys. Chem. B* **2009**, *113*, 14779−14786.
(18) Peduto, A.; Pagano, B.; Petronzi, C.; Massa, A.; Esposito, V.; Virgilio, A.; Paduano, F.; Trapasso, F.; Fiorito, F.; Florio, S.; Giancola, C.; Galeone, A.; Filosa, R. Design, synthesis, biophysical and biological studies of trisubstituted naphthalimides as G-quadruplex ligands. *Bioorg. Med. Chem.* **2011**, *19*, 6419−6429.
(19) Thiriet, C.; Hayes, J. J. Chromatin in need of a fix: Phosphorylation of H2AX connects chromatin to DNA repair. *Mol. Cell* **2005**, *18*, 617−622.
(20) Takai, H.; Smogorzewska, A.; de Lange, T. DNA damage foci at dysfunctional telomeres. *Curr. Biol.* **2003**, *13*, 1549−1556.
(21) Morris, G. M.; Huey, R.; Lindstrom, W.; Sanner, M. F.; Belew, R. K.; Goodsell, D. S.; Olson, A. J. AutoDock4 and AutoDockTools4: Automated docking with selective receptor flexibility. *J. Comput. Chem.* **2009**, *30*, 2785−2791.
(22) Evans, D. A.; Neidle, S. Virtual screening of DNA minor groove binders. *J. Med. Chem.* **2006**, *49*, 4232−4238.
(23) Cornell, W. D.; Cieplak, P.; Bayly, C. I.; Gould, I. R.; Merz, K. W., Jr.; Ferguson, D. M.; Spellmeyer, D. C.; Fox, T.; Caldwell, J. W.; Kollman, P. A. A Second Generation Force Field for the Simulation of Proteins, Nucleic Acids, and Organic Molecules. *J. Am. Chem. Soc.* **1995**, *117*, 5179−5197.
(24) (a) Hwang, T. L.; Shaka, A. J. Water suppression that works. Excitation sculpting using arbitrary waveforms and pulsed field gradients. *J. Magn. Reson. A* **1995**, *112*, 275−279. (b) Dalvit, C. Efficient multiple-solvent suppression for the study of the interactions of organic solvents with biomolecules. *J. Biomol. NMR* **1998**, *11*, 437−444.
(25) Salvati, E.; Scarsella, M.; Porru, M.; Rizzo, A.; Iachettini, S.; Tentori, L.; Graziani, G.; D'Incalci, M.; Stevens, M. F.; Orlandi, A.; Passeri, D.; Gilson, E.; Zupi, G.; Leonetti, C.; Biroccio, A. PARP1 activated at telomeres upon G4 stabilization: possible target for telomere-based therapy. *Oncogene* **2010**, *29*, 6280−6293.
(26) Biroccio, A.; Amodei, S.; Benassi, B.; Scarsella, M.; Cianciulli, A.; Mottolese, M.; Del Bufalo, D.; Leonetti, C.; Zupi, G. Reconstitution of hTERT restores tumorigenicity in melanoma-derived c-Myc low-expressing clones. *Oncogene* **2002**, *21*, 3011−3019.
(27) Biroccio, A.; Benassi, B.; Filomeni, G.; Amodei, S.; Marchini, S.; Chiorino, G.; Rotilio, G.; Zupi, G.; Ciriolo, M. R. Glutathione influences c-Myc-induced apoptosis in M14 human melanoma cells. *J. Biol. Chem.* **2002**, *277*, 43763−43770.